Equiphase-sphere approximation for light scattering by stochastically inhomogeneous microparticles

Xu Li

Department of Biomedical Engineering, Northwestern University, Evanston, Illinois 60208, USA

Zhigang Chen and Allen Taflove

Department of Electrical and Computer Engineering, Northwestern University, Evanston, Illinois 60208, USA

Vadim Backman

Department of Biomedical Engineering, Northwestern University, Evanston, Illinois 60208, USA

(Received 26 May 2004; published 17 November 2004)

We report the development and validation of the equiphase-sphere (EPS) approximation for calculating the total-scattering cross-section (TSCS) spectra of inhomogeneous microparticles having complex interior structures. We show that this closed-form, analytical approximation can accurately model the TSCS of randomly inhomogeneous spherical particles having internal refractive index variations with geometrical scales spanning from nanometers (i.e., subwavelength) to microns (i.e., suprawavelength). Moreover, we derive an easy-to-use criterion for the range of validity of the EPS approximation in modeling TSCS of inhomogeneous particles. The work discussed in this paper may positively impact tissue optical imaging and diagnostic applications.

I. INTRODUCTION

Examples of inhomogeneous particles range from mineral particles and atmospheric aerosols to cell nuclei in biological tissue. Characterizing the light-scattering properties of these particles is important for a variety of applications in atmospheric science, oceanography, astronomy, and biomedical optics [1].

Analytical methods capable of accurately modeling light scattering by inhomogeneous particles have been developed for only a small set of particle geometries, such as the concentrically stratified sphere [2] and sphere with spherical inclusions [3]. However, naturally occurring particles usually have much more complex shapes and internal structures. For such particles, approximation methods are desirable for providing practical solutions to light-scattering problems. However, despite significant interest in the development of approximation methods for characterizing the light-scattering properties of inhomogeneous and nonspherical particles, satisfactory results have not been achieved. The complexity of this problem is illustrated by a quote from Bohren in his chapter on light scattering in Ref. [26], "This search resembles that for the Holy Grail—and has been as fruitless."

Recently, we have investigated the light-scattering properties of inhomogeneous spherical particles having an internal refractive index *n*, assigned as an uncorrelated random variable to uniformly sized cubic subvolumes within each particle [4]. Numerical experiments using high-resolution finite-difference-time-domain (FDTD) computational electrodynamics models [5] and supporting analyses demonstrated that the spectral dependence of the total-scattering cross section (TSCS) of such a particle can closely resemble that of its homogeneous, volume-averaged counterpart if the size of each cubic subvolume inhomogeneity within the original particle is sufficiently small relative to the optical wavelength.

In this paper, we advance beyond the simple uncorrelated particle inhomogeneity considered in [4], and report a closed-form analytical approximation that provides accurate TSCS spectra characterization despite the internal complexity of the particle. Specifically, the particles considered here are spheres that have internal distributions of a refractive index synthesized using the isotropic Gaussian random field (GRF) model. GRF models have been used previously to characterize the morphology of randomly inhomogeneous materials and characterizing complex microstructures [6], accounting for many features observed in naturally occurring random media. For such an assignment of a refractive index, we demonstrate that the equiphase-sphere (EPS) approximation introduced in Refs. [7–9] provides an accurate closed-form calculation of the TSCS spectra of highly inhomogeneous particles having GRF refractive index variations with geometrical scales spanning nanometers to microns. Moreover, using the Wentzel-Kramers-Brillouin (WKB) technique, we derive the validity range of the EPS approximation as a function of the statistical parameters of the interior refractive index distribution. In all cases reported in this paper, validation studies are conducted using high-resolution FDTD simulations that model particles having a wide range of standard deviations and correlation lengths for the internal refractive-index distribution.

II. REVIEW OF THE EPS APPROXIMATION FOR LIGHT SCATTERING BY MICROPARTICLES

We recently introduced the EPS approximation for calculating the TSCS spectra of nonspherical particles with sizes in the resonance range [7–9]. Using a simple expression, this method explicitly links the size and shape parameters of nonspherical particles to the oscillation feature in their TSCS spectra.

In the EPS approximation, the wavelength-dependent TSCS spectrum of a particle is given by the sum of the "edge-effect" term $\sigma_s^{(s)}(\lambda)$ and the, "volume-diffraction-effect" term $\sigma_s^{(v)}(\lambda)$ [7]

$$\sigma_s(\lambda) = \sigma_s^{(s)}(\lambda) + \sigma_s^{(v)}(\lambda). \tag{1}$$

Here, when the high frequency ripples resulting from interference of the surface waves is neglected, $\sigma_s^{(s)}(\lambda)$ can be approximated as [7,10]

$$\sigma_s^{(s)}(\lambda) \approx 2S[2\pi(3V/4\pi)^{1/3}/\lambda]^{-2/3}, \tag{2}$$

where S is the particle's maximum cross-section area transverse to the direction of the incident light, and V is the volume of the particle.

For a particle with $2\pi d(n-1)/\lambda \gg 1$ and $(n-1) < 1$, where d is the mean diameter and n is the refractive index, the volume term $\sigma_s^{(v)}(\lambda)$ can be approximated using the WKB technique [11]

$$\sigma_s^{(v)}(\lambda) = 2\,\mathrm{Re}\left(\int\int_S \{1 - \exp[i\xi(\mathbf{r}')]\}d^2\mathbf{r}'\right), \tag{3}$$

where $\mathbf{r}'$ is a position vector in the plane orthogonal to the direction of propagation of the incident wave and $\xi(\mathbf{r}')$ is the phase shift of a light ray crossing plane S at position $\mathbf{r}'$. $\xi(\mathbf{r}')$ is expressed as

$$\xi(\mathbf{r}') = (2\pi/\lambda)\int_{L(\mathbf{r}')} [n(l(\mathbf{r}')) - 1]dl, \tag{4}$$

where $L(\mathbf{r}')$ is the path of the light ray crossing $\mathbf{r}'$. For a homogeneous spherical particle with refractive index n_0,

$$L = d[1 - \sin^2\gamma(\mathbf{r}')/n_0^2]^{1/2}, \tag{5}$$

where γ is the angle between the incident-ray propagation direction and the radial vector pointing from the center of the particle. After performing the integration in Eq. (3), $\sigma_s^{(v)}(\lambda)$ for a homogeneous spherical particle is given by

$$\sigma_s^{(v)}(\lambda) = 2S[1 - 2n_0\sin\rho/\rho + 4n_0\sin^2(\rho/2)/\rho^2], \tag{6}$$

where $\rho = 2\pi d(n_0 - 1)/\lambda$ is the maximum phase shift produced by the homogeneous sphere.

We note Eq. (6) becomes equivalent to the van de Hulst approximation [12]

$$\sigma_s(\lambda) = 2S[1 - 2\sin\rho/\rho + 4\sin^2(\rho/2)/\rho^2] \tag{7}$$

for spheres with low refractive indexes. The most distinctive feature that can be observed from both Eqs. (6) and (7) is the "interference structure" [13], which refers to slow oscillations of TSCS as a function of wavelength with the frequency of these oscillations proportional to the diameter of the particle. With sufficiently large ρ, the higher order term $\sin^2(\rho/2)/\rho^2$ can be neglected; thus the diameter of the particle can be easily derived from the oscillation frequency by $d = \lambda_1\lambda_2/(\lambda_2 - \lambda_1)/(n_0 - 1)$, where λ_1 and λ_2 are wavelengths corresponding to two adjacent maxima or minima in the TSCS spectrum. In addition, by including a surface term [Eq. (2)] and implicitly incorporating the refraction effect on the

direction of the light-ray propagation [Eq. (5)], the formulas given by Eqs. (1), (2), and (6) provide improved accuracy for calculating the TSCS spectra, particularly for particles with higher refractive indices.

Motivated by the questions whether the interference structures are preserved for nonspherical particles, and how their TSCS spectra are associated with the particle size and shape characteristics, we previously introduced the concept of the "equiphase sphere" [7]. Most recently, we proposed to use the equiphase-sphere (EPS) approximation [Eqs. (1), (2), and (6)] to calculate the TSCS spectra of a variety of nonspherical particles [8,9], where ρ is replaced by the equivalent maximum phase shift calculated according to the particle's geometrical characteristics.

III. APPLICATION OF EPS THEORY TO THE INHOMOGENEOUS SPHERES: RANGE OF VALIDITY

In this section we focus our discussion on applying the EPS approximation to spherical particles with inhomogeneous interior refractive index. Here, ρ of Eq. (6) is simply replaced by the maximum phase shift produced by the homogeneous counterpart of the particle with n_0 equal to the volume-averaged refractive index of the inhomogeneous particle. Upon this substitution, Eq. (6) predicts that the oscillation features in the TSCS spectrum of an inhomogeneous particle follow that of its homogeneous counterpart with a volume-averaged refractive index.

In order to apply the EPS method in practice, it is important to determine the validity conditions of this approximation. We now investigate how the internal refractive-index distribution affects the validity and accuracy of the EPS approximation applied to inhomogeneous particles. The derivation of an analytical validity condition for Eq. (3) is summarized below.

The validity analysis of the EPS approximation is based on the WKB technique [Eq. (3)] from which Eq. (6) is derived. For an inhomogeneous spherical particle, the relative phase shift $\xi(\mathbf{r}')$ can be expressed as $\xi(\mathbf{r}') = \xi_0(\mathbf{r}') + \delta\xi(\mathbf{r}')$. Here, $\xi_0(\mathbf{r}') = 2\pi(n_0 - 1)L(\mathbf{r}')/\lambda$ is the phase shift of a light ray propagating through the homogeneous counterpart of the particle. The term $\delta\xi(\mathbf{r}')$ accounts for the phase-shift difference due to refractive-index inhomogeneity. If

$$\delta\xi(\mathbf{r}') < \pi/2, \tag{8}$$

the exponent in Eq. (3) can be expanded to perform the integration analytically. This yields

$$\sigma_s^{(v)} \approx \sigma_{n_0}^{(v)} + \delta\sigma^{(v)}, \tag{9}$$

where $\sigma_{n_0}^{(v)}(\lambda) = 2S[1 - 2n_0\sin\rho/\rho + 4n_0\sin^2(\rho/2)/\rho^2]$ is the scattering produced by the equiphase-sphere counterpart of the particle, and $\delta\sigma^{(v)}$ is the error term produced by refractive-index inhomogeneity. The EPS approximation is valid provided that $\delta\sigma^{(v)} \ll \sigma_{EPS}^{(v)}$.

We point out that the expansion in Eq. (9) depends on condition (8). Thus, we shall examine the inequality (8) in detail. The phase shift error $\delta\xi(\mathbf{r}')$ due to inhomogeneity is given by
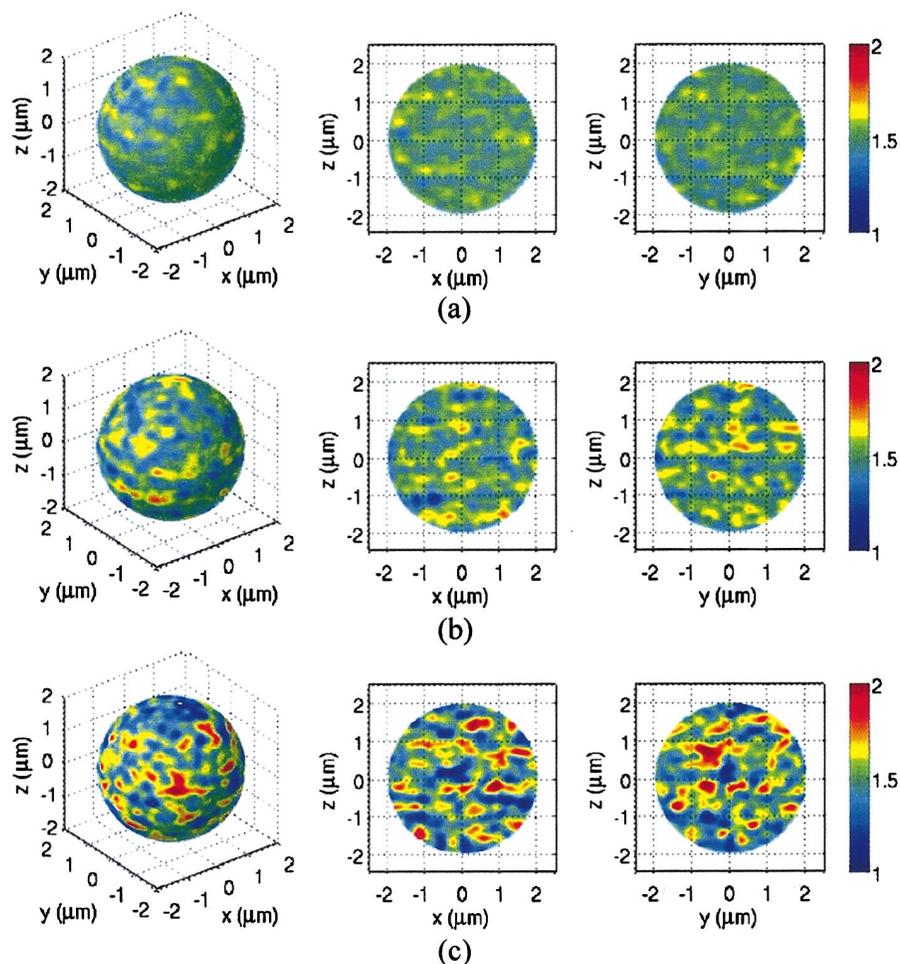
FIG. 1. (Color) Examples of inhomogeneous spherical particles having GRF refractive-index distributions with fixed $n_0 = 1.5$ and $L_c = 400$ nm, but increasing standard deviations: (a) $\sigma_n = 0.05$, (b) $\sigma_n = 0.098$, (c) $\sigma_n = 0.163$.

$$\delta\xi(\mathbf{r}') = \int_{L(\mathbf{r})} \frac{2\pi}{\lambda} \delta n(\mathbf{r}', l) dl, \tag{10}$$

where $\delta n(\mathbf{r}', l)$ denotes the refractive-index fluctuation from its volume average at position $(\mathbf{r}', l)$. If the spatial distribution of the refractive index has a correlation length L_c, then Eq. (10) can be approximated by the sum $\delta\xi(\mathbf{r}') \approx (2\pi/\lambda)\Sigma_{i=1}^{N}\delta n_i L_c$. Furthermore, if $n(\mathbf{r})$ is a stochastic function with a probability density function characterized by a standard deviation σ_n, $\delta\xi(\mathbf{r}')$ can be approximated as

$$\delta\xi(\mathbf{r}') \approx 2\pi L_c \sqrt{N} \sigma_n/\lambda \lesssim 2\pi\sqrt{L_c d}\sigma_n/\lambda. \tag{11}$$

Therefore, the inequality (5) is replaced by

$$\beta \equiv 4\sqrt{L_c d}\sigma_n/\lambda < 1. \tag{12}$$

Note that the parameter β quantifies the most probable maximum phase shift error $\delta\xi(\mathbf{r}')$ in an inhomogeneous particle with a stochastic distribution of its refractive index. If $\beta \ll 1$, this phase error is negligible, and therefore EPS approximation gives accurate estimate of the TSCS spectrum of the inhomogeneous particle. On the other hand, when $\beta \ll 1$, the expansion (9) may not be performed. In this case, EPS approximation may give erroneous results. We also note that β is proportional to the square root of L_c. This indicates that refractive index fluctuations within larger geometrical scales

have more significant impact on the accuracy of the EPS approximation.

IV. GAUSSIAN RANDOM FIELD MODEL FOR INHOMOGENEOUS REFRACTIVE INDEX DISTRIBUTION

In order to investigate light scattering by particles with a wide variety of shapes and interior structures, statistical approaches are very useful for modeling the particle geometry [14]. In particular, the Gaussian random sphere has been successfully used as a geometric model to study light scattering by irregularly shaped nonspherical particles [15]. In this section, we describe how to use the Gaussian random field (GRF) model to synthesize the stochastic distribution of the refractive index within inhomogeneous particles.

Three-dimensional (3D) GRFs are analogs of one-dimensional stochastic processes having a Gaussian probability density function. Here, we consider the refractive index $n(\mathbf{r})$ as a function of spatial location $\mathbf{r} = (x, y, z)$. Each value of $n(\mathbf{r})$ is a Gaussian random variable with mean $n_0 = \langle n(\mathbf{r})\rangle$ and standard deviation $\sigma_n = \sqrt{\langle[n(\mathbf{r}) - n_0]^2\rangle}$. For a GRF model with unit standard deviation, the two-point correlation function $C_n(r)$ is defined as
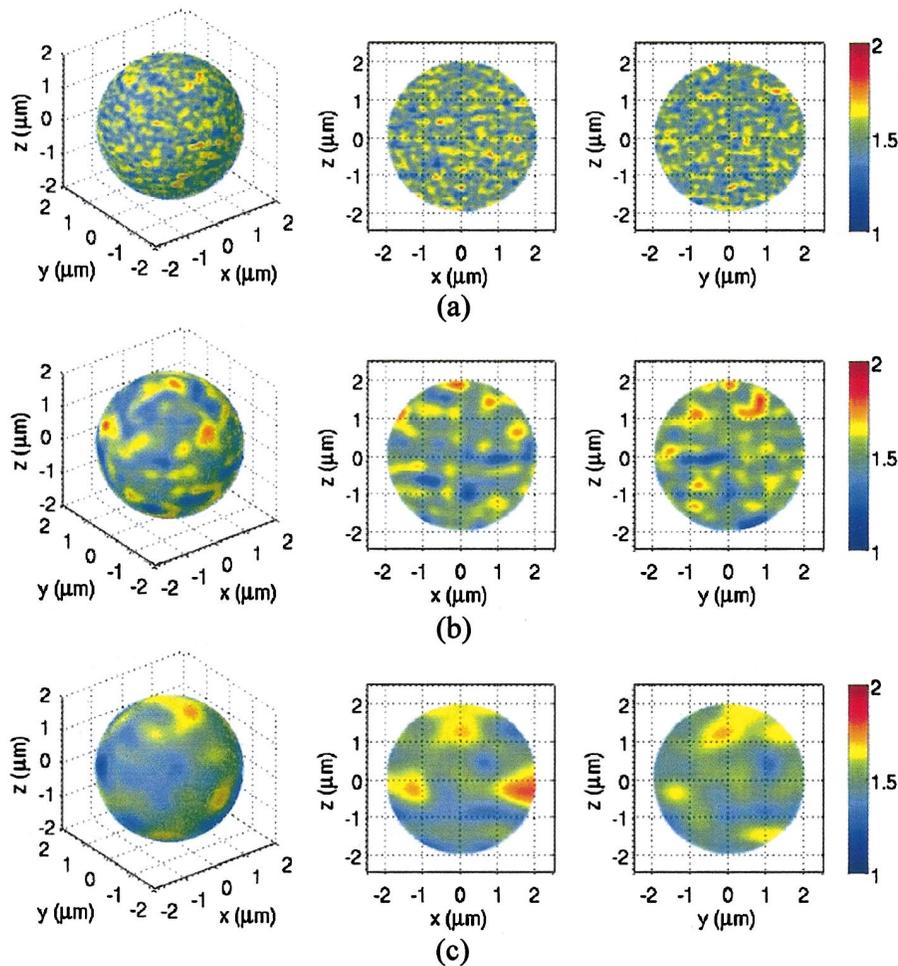
FIG. 2. (Color) Examples of inhomogeneous spherical particles having fixed $n_0 = 1.5$ and $\sigma_n \approx 0.1$ but with increasing correlation lengths. (a) $L_c = 100$ nm, (b) $L_c = 600$ nm, (c) $L_c = 1.2$ μm.

$$C_n(r) = \langle [n(0) - n_0][n(r) - n_0] \rangle, \qquad (13)$$

where $r = |\mathbf{r}|$. In this paper, we use the Gaussian function as the correlation model

$$C_n(r) = e^{-r^2/(L_c/2)^2}, \qquad (14)$$

where L_c is the characteristic correlation length representing the length scale over which the correlation drops to a negligible level. For such a choice of correlation function, the statistics of the spatial distribution of $n(\mathbf{r})$ is uniquely determined by the parameter L_c. If $L_c \rightarrow \infty$, we have $C_n(r) \equiv 1$ and the resulting spatial distribution is homogeneous. Lower L_c corresponds to refractive-index fluctuations in smaller geometric scales.

Various methods can be used to generate realizations of the GRF model. In this paper, we have adopted the turning-band method [16], where the 3D realizations of the GRF model are generated by summing independent realizations of one-dimensional random functions with directional vectors uniformly distributed over the unit sphere. Using this method, we create geometrical models of spherical particles with the refractive index having GRF distributions.

Figures 1(a)–1(c) graph shows sample inhomogeneous spherical particles with fixed $n_0 = 1.5$ and correlation length $L_c = 400$ nm, but increasing standard deviations ranging from $\sigma_n = 0.05$ [Fig. 1(a)] to $\sigma_n = 0.163$ [Fig. 1(c)]. In each figure, the particle refractive-index distribution is depicted in the 3D view of a surface plot (left panel), a cross-sectional cut in the $\hat{x}$-$\hat{z}$ plane (middle panel), and a cross-sectional cut in the $\hat{y}$-$\hat{z}$ plane (right panel). Each colormap of the particle interior illustrates the spatial distribution of the particles' refractive indices. The corresponding scale of the variation is illustrated using the colorbars displayed on the right in each figure. We note that the exact geometry of the refractive-index spatial distribution is unique for each case since the stochastic method is used in randomly generating these geometries. However, since the three particles all have the same correlation length $L_c = 400$ nm, their spatial refractive-index distributions have fluctuations on the same geometrical scale. It is also evident that the standard deviation σ_n determines the magnitude of the refractive-index fluctuation. For example, for the particle shown in Fig. 1(c), the standard deviation $\sigma_n = 0.163$ results in refractive-index fluctuations raging approximately from 1.0 to 2.0.

Figure 2 shows sample inhomogeneous spherical particles with fixed $n_0 = 1.5$ and $\sigma_n \approx 0.1$ but L_c increasing from 100 nm [Fig. 2(a)] to 1.2 μm [Fig. 2(c)]. These examples demonstrate the capability of the GRF model to mimic refractive-index fluctuations occurring over a wide range of
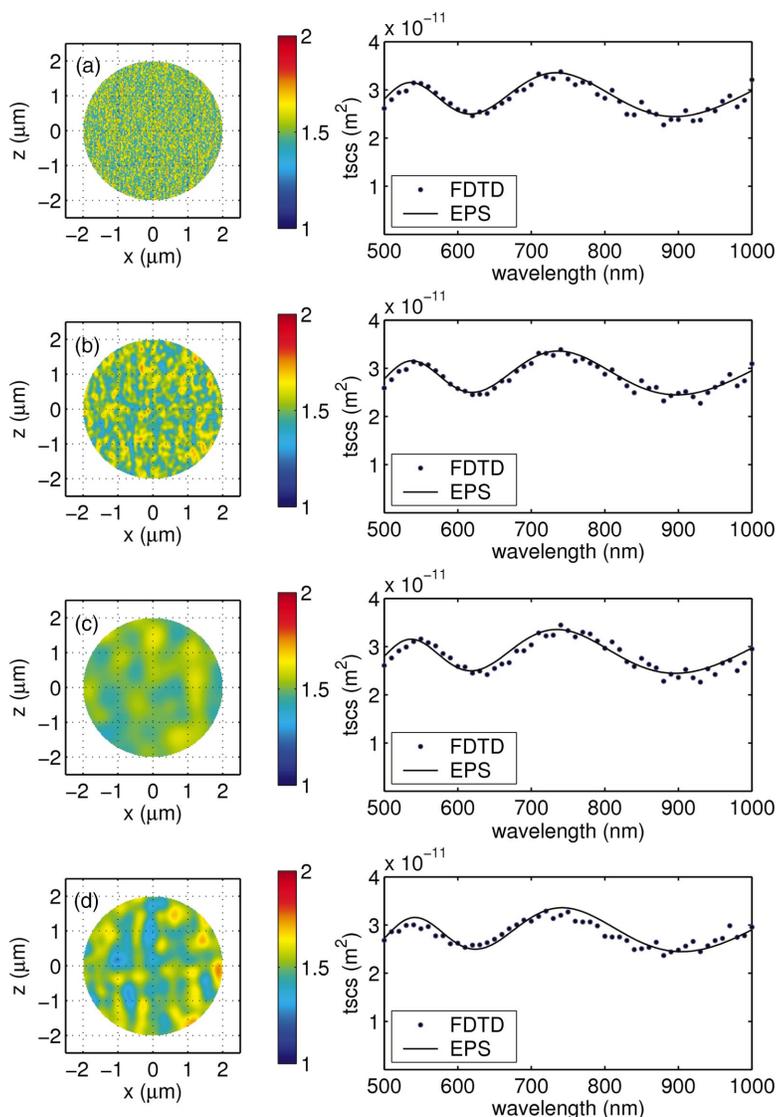
FIG. 3. (Color) Comparison of TSCS spectra calculated using rigorous FDTD numerical modeling and EPS analyses. The spatial distribution of the particle refractive index in the $\hat{x}$-$\hat{z}$ cross-sectional cut is displayed in the left panel. (a) $\sigma_n=0.1$, $L_c=50$ nm, $\beta=0.36$. (b) $\sigma_n=0.08$, $L_c=100$ nm, $\beta=0.40$. (c) $\sigma_n=0.05$, $L_c=1$ μm, $\beta=0.78$. (d) $\sigma_n=0.08$, $L_c=600$ nm, $\beta=0.97$. Good agreement is observed between the EPS-calculated TSCS spectra and the FDTD benchmarks since $\beta<1$.

geometrical scales appropriate for simulation of natural particles.

V. NUMERICAL VALIDATION OF THE EPS APPROXIMATION AND ITS EXPECTED RANGE OF VALIDITY

We now describe our validation of the EPS approximation discussed in Secs. II and III. To this end, we have conducted a series of numerical experiments that compared TSCS spectra calculated using the EPS approximation with numerical FDTD benchmark data for a wide variety of inhomogeneous spherical particles such as shown in Figs. 1 and 2. This comparison permits us to validate the EPS approximation and to explore the correlation between the approximation accuracy and the geometric characteristics of the refractive-index distribution.

The FDTD method has been shown to be a robust means to numerically solve the Maxwell's equations in studies of light scattering problems [17]. We used a staircasing scheme with 25-nm resolution to sample the refractive-index spatial variations of interest. Following the same procedures as described in our previous work [9], we calculated TSCS spectra of ($n_0=1.5$, $d=4$ μm) spherical particles ranging from slightly inhomogeneous ($1.45 \leqslant n \leqslant 1.55$) to highly inhomogeneous ($1.0 \leqslant n \leqslant 2.0$). The numerical experiments include a wid range of geometrical scales of interior refractive-index fluctuations with L_c ranging from 50 nm to 1.2 μm.

Figure 3 shows four representative results of our numerical experiments. In each example, the spatial distribution of the particle refractive index in one cross-sectional cut is displayed on the left, and the TSCS spectra calculated with FDTD and the EPS approximation are graphed on the right. We note that although these inhomogeneous particles have a variety of values of σ_n and L_c, the validity condition $\beta \equiv 4\sqrt{L_c d}\sigma_n/\lambda < 1$ is satisfied for all four cases. Indeed, the TSCS spectra calculated by the EPS approximation very well matched the benchmark data provided by FDTD for all four cases.

As L_c or σ_n of the interior refractive-index distribution become greater, the accuracy of the EPS approximation is expected to decline. This effect is illustrated in Fig. 4. For these four particles with increasing β, the EPS-calculated TSCS spectra progressively deviate from the FDTD data. In
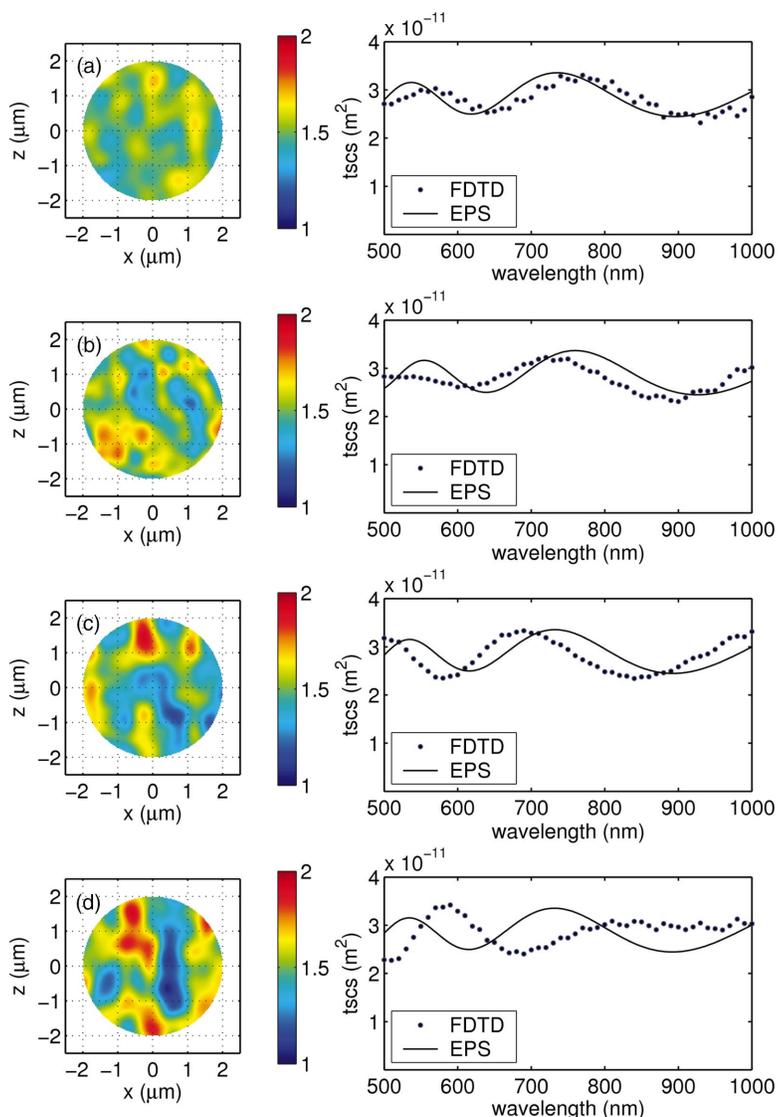
FIG. 4. (Color) Comparison of TSCS spectra calculated using FDTD modeling and the EPS approximation for particles with large σ_n or L_c. (a) $\sigma_n=0.08$, $L_c=1.0$ μm, $\beta=1.29$. (b) $\sigma_n=0.13$, $L_c=800$ nm, $\beta=1.90$. (c) $\sigma_n=0.15$, $L_c=1.0$ μm, $\beta=2.32$. (d) $\sigma_n=0.16$, $L_c=1.0$ μm, $\beta=2.61$. As β increases well above 1, the EPS calculated TSCS spectra progressively deviate from the FDTD benchmarks.

an extreme case shown in Fig. 4(d), where both the magnitude and geometrical scale of the refractive-index inhomogeneity are large ($1.0 \leqslant n \leqslant 2.0$, $L_c=1.0$ μm, and $\beta=2.6$), the oscillatory period of the TSCS spectrum calculated by the EPS approximation completely departs from the FDTD benchmark data.

We summarize our numerical experiments with a parametric study to demonstrate the impact of the statistical parameters of refractive-index distribution (characterized by the β factor) on the validity and accuracy of the EPS method. We used two complimentary parameters, the rms error R and the correlation coefficient r_c to quantify the accuracy of the approximate EPS-calculated TSCS spectra with respect to the exact FDTD benchmark data. The rms error measures the overall estimation accuracy, while the correlation coefficient, which is defined as

$$r_c \equiv \frac{\langle[\mathit{tscs}_{FDTD}(\lambda_i) - \langle\mathit{tscs}_{FDTD}(\lambda)\rangle][\mathit{tscs}_{EPS}(\lambda_i) - \langle\mathit{tscs}_{EPS}(\lambda)\rangle]\rangle}{\sigma[\mathit{tscs}_{FDTD}(\lambda)]\sigma[\mathit{tscs}_{EPS}(\lambda)]}, \tag{15}$$

measures the capability of the EPS approximation to replicate the oscillation characteristics of the TSCS spectrum.

Figure 5 plots the rms error R and the correlation coefficient r_c as functions of β for 26 inhomogeneous spheres covering a wide variety of refractive index distributions (L_c ranging from 50 nm to 1.2 μm and σ_n ranging from 0.02 to 0.163). In order to better illustrate the connection between the quality of the EPS approximation and the accuracy mea-
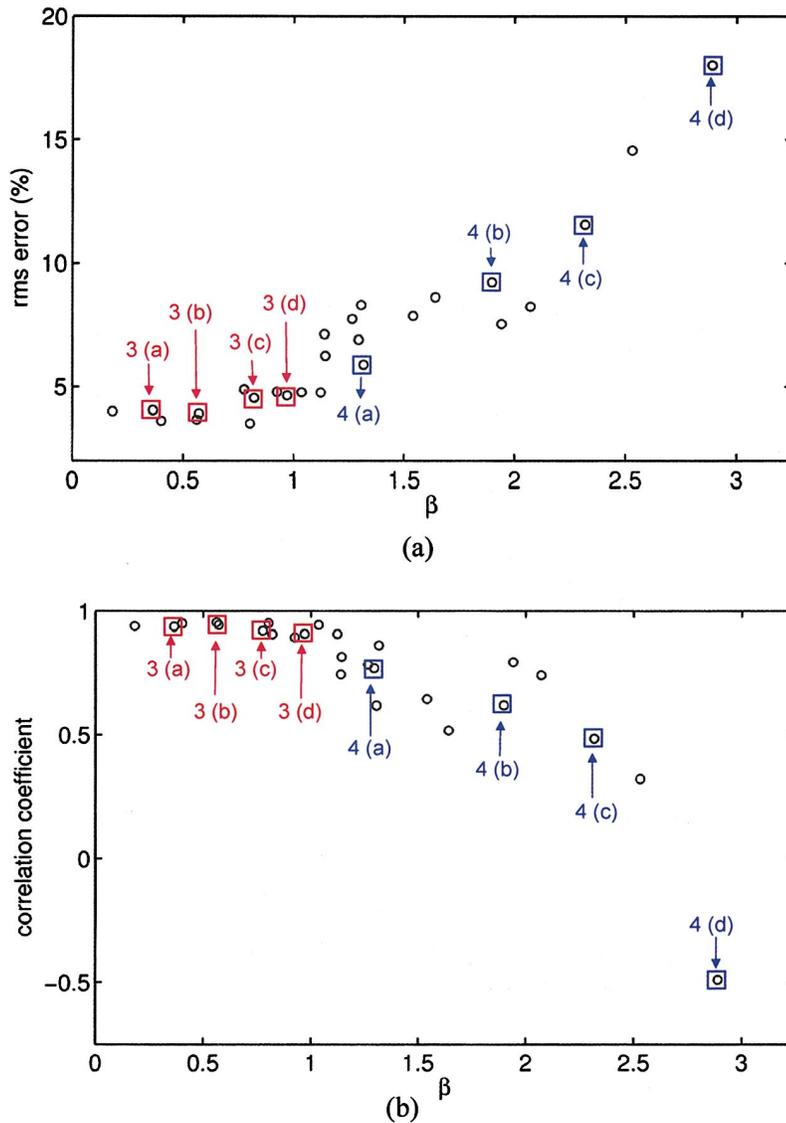
FIG. 5. (Color) Accuracy measures of the EPS approximation of the TSCS spectrum as functions of the validity-condition parameter β for 26 cases of inhomogeneous spheres covering 50 nm $< L_c <$ 1.2 μm and 0.02 $< \sigma_n <$ 0.163. In all cases, FDTD simulation results are used as the benchmark data. (a) rms error (%) vs β. (b) Correlation coefficient vs β. When $\beta < 1$, the rms error is less than 5% and the correlation coefficient is greater than 0.9.

sures, we cross-reference eight data points in Figs. 5(a) and 5(b) with their corresponding particle geometries and TSCS spectra shown in Fig. 3 and Fig. 4.

We observe from Fig. 5 that when criterion (9) is satisfied ($\beta < 1$), the EPS approximation is sufficiently accurate, i.e., $r_c \geq 0.9$ and $R < 5\%$. It is also evident from Fig. 5(a) that when $\beta > 1$, the accuracy of the EPS approximation degrades rapidly as β increases. This further demonstrates the importance of the β parameter in determining the validity of the EPS approximation.

VI. SUMMARY AND DISCUSSION

We have presented the development and validation of the equiphase-sphere (EPS) approximation for the total-scattering cross-section (TSCS) spectra of inhomogeneous spherical particles having complex interior structures. We have shown that the closed-form, analytical approximation can accurately model the TSCS of randomly inhomogeneous spherical particles having internal refractive index variations with geometrical scales spanning from nanometers (i.e., sub-wavelength) to microns (i.e., suprawavelength). An easy-to-use criterion for the range of approximation validity has been provided to guide the practical application of this method.

Although not limited to a single category of applications, the work discussed here may positively impact tissue optical imaging and diagnostic applications. It is recognized that the analysis of spectral, angular, and other characteristics of light scattered from living tissue can provide valuable diagnostic information [18–25]. Due to the complexity in the microarchitecture of biological tissue, the understanding of light scattering by particles with complex shapes and interior structure is of great importance for the future refinement of the current optical techniques. Importantly, the development of methods such as the EPS approximation to analyze tissue light scattering will enable gathering new accurate information about tissue organization and its alteration in disease. In turn, these insights can be further used for disease diagnosis

as well as the biological understanding of tissue pathophysiology. In our future work, we shall focus on developing effective techniques for analyzing the angular-dependent and backward scattering properties of biologically relevant particles.

[1] M. I. Mishchenko, J. W. Hovenier, and L. D. Travis, *Light Scattering by Nonspherical Particles: Theory, Measurements and Applications* (Academic, San Diego, CA, 2000).

[2] R. Bhandari, Appl. Opt. **24**, 1960 (1985).

[3] K. A. Fuller, J. Opt. Soc. Am. A Opt. Image Sci. Vis **12**, 893 (1995).

[4] Z. Chen, A. Taflove, and V. Backman, Opt. Lett. **28**, 765 (2003).

[5] A. Taflove and S. Hagness, *Computational Electrodynamics: The Finite-Difference Time-Domain Method* (Artech, Boston, 2000).

[6] R. J. Adler, *The Geometry of Random Fields* (Wiley, New York, 1981).

[7] Z. Chen, A. Taflove, and V. Backman, J. Opt. Soc. Am. A **20**, 88 (2004).

[8] X. Li, Z. Chen, J. Gong, A. Taflove, and V. Backman, Opt. Lett. **29**, 1239 (2004).

[9] X. Li, Z. Chen, A. Taflove, and V. Backman, Appl. Opt. **43**, 4497 (2004).

[10] H. Nussenzveig and W. Wiscombe, Phys. Rev. Lett. **45**, 1490 (1980).

[11] J. D. Klett and R. A. Sutherland, Appl. Opt. **31**, 373 (1992).

[12] H. C. v. d. Hulst, *Light Scattering by Small Particles* (Dover, New York, 1981).

[13] P. Chylek and J. Zhan, J. Opt. Soc. Am. A **6**, 1846 (1989).

[14] K. Muinonen, in *Light Scattering by Nonspherical Particles: Theory, Measurements, and Applications*, edited by M. I. Mishchenko, J. W. Hovenier, and L. D. Travis (Academic, San Diego, 2000).

[15] K. Muinonen, T. Nousiainen, K. Lumme, P. Fast, and J. I. Peltoniemi, J. Quant. Spectrosc. Radiat. Transf. **55**, 577 (1996).

[16] G. Matheron, Adv. Appl. Probab. **5**, 439 (1973).

[17] A. Dunn and R. Richards-Kortum, IEEE J. Sel. Top. Quantum Electron. **2**, 898 (1996).

[18] B. J. Tromberg, R. C. Haskell, S. J. Madsen, and L. O. Svaasand, Comments Mol. Cell. Biophys. **8**, 359 (1995).

[19] A. Yodh and B. Chance, Phys. Today **48**, 34 (1995).

[20] A. Wax, C. Yang, and J. A. Izatt, Opt. Lett. **28**, 1230 (2003).

[21] J. W. Pyhtila, R. N. Graf, and A. Wax, Opt. Express **11**, 3473 (2003).

[22] L. T. Perelman, V. Backman, M. Wallace, G. Zonios, R. Manoharan, A. Nusrat, S. Shields, M. Seiler, C. Lima, T. Hamano, I. Itzkan, J. V. Dam, J. M. Crawford, and M. S. Feld, Phys. Rev. Lett. **80**, 627 (1998).

[23] Y. L. Kim, Y. Liu, R. K. Wali, H. K. Roy, M. J. Goldberg, A. K. Kromine, K. Chen, and V. Backman, IEEE J. Sel. Top. Quantum Electron. **9**, 243 (2003).

[24] H. K. Roy, Y. Liu, R. Wali, Y. L. Kim, A. K. Kromine, M. J. Goldberg, and V. Backman, Gastroenterology **126**, 1071 (2004).

[25] J. R. Mourant, T. M. Johnson, S. Carpenter, A. Guerra, T. Aida, and J. P. Freyer, J. Biomed. Opt. **7**, 378 (2002).

[26] C. F. Bohren, *Handbook of Optics*, 2nd ed., edited by M. Bass (McGraw-Hill, New York, 1995).